

UNIVERSITY of CALIFORNIA  
SANTA CRUZ

**SEARCHES OF RHESSI DATA FOR WEAK SIGNALS ASSOCIATED  
WITH TERRESTRIAL GAMMA-RAY FLASHES**

A thesis submitted in partial satisfaction of the  
requirements for the degree of

BACHELOR OF SCIENCE

in

APPLIED PHYSICS

by

**Paul R. Buzbee**

26 April 2013

The thesis of Paul R. Buzbee is approved by:

---

Professor David M. Smith  
Advisor

---

Professor David P. Belanger  
Theses Coordinator

---

Professor Michael Dine  
Chair, Department of Physics

Copyright © by  
Paul R. Buzbee  
2013

## Abstract

Searches of RHESSI Data for Weak Signals Associated with Terrestrial Gamma-Ray  
Flashes

by

Paul R. Buzbee

Terrestrial gamma-ray flashes (TGFs) are short intense bursts of gamma-rays associated with lightning. The NASA Reuven Ramaty High Energy Solar Spectroscopic Imager (RHESSI) satellite has detected hundreds of TGFs. Here we present three separate analyses of RHESSI data. First, we look for reflected echoes of electron beams in regions of weaker magnetic field strength. By stacking the gamma-ray time profiles of the eleven candidates at the estimated return time, we observe a peak of probability  $4.53 \times 10^{-6}$ . We conclude that five of the candidates are returned electron beams. Secondly, we present the current progress on building a third catalog of RHESSI TGFs by expanding on the work of the previous two. Finally, we present the results of summing gamma-ray time profiles associated with nearby lightning strikes from the World Wide Lightning Location Network (WWLLN), and establish a strict upper limit on the average gamma-ray flux RHESSI receives from lightning,  $6.20 \times 10^{-4}$ , as a fraction of an average RHESSI TGF.

# Contents

<b>List of Figures</b>	<b>vi</b>
<b>List of Tables</b>	<b>vii</b>
<b>Dedication</b>	<b>viii</b>
<b>Acknowledgements</b>	<b>ix</b>
<b>1 Introduction</b>	<b>1</b>
1.1 Mechanism of a TGF . . . . .	2
1.2 RHESSI . . . . .	5
<b>2 Electron beam reflections</b>	<b>8</b>
2.1 Introduction: Motion of electrons in the magnetosphere . . . . .	8
2.2 Methods . . . . .	10
2.2.1 Restrictions . . . . .	10
2.2.2 Simulations . . . . .	11
2.2.3 Stacked alignment . . . . .	12
2.3 Results . . . . .	12
2.4 Discussion . . . . .	15
<b>3 Building a new RHESSI TGF catalog</b>	<b>16</b>
3.1 Introduction . . . . .	16
3.2 Methods . . . . .	17
3.2.1 Approach . . . . .	17
3.2.2 Stage 1 . . . . .	17
3.2.3 Stage 2 . . . . .	18
3.2.4 Adjusting Thresholds . . . . .	20
3.3 Results . . . . .	24
3.4 Discussion . . . . .	25
3.4.1 Future Work . . . . .	25
<b>4 Using WWLLN to search for sub-luminous TGFs</b>	<b>27</b>
4.1 Introduction . . . . .	27
4.2 Methods . . . . .	28
4.2.1 Finding Nearby Strikes . . . . .	28
4.2.2 Processing RHESSI data . . . . .	28
4.3 Results . . . . .	30
4.4 Discussion . . . . .	31
<b>5 Conclusions</b>	<b>34</b>



# List of Figures

1.1	Map of TGFs and lightning . . . . .	2
1.2	Relativistic runaway . . . . .	3
1.3	Geometry of a TGF event . . . . .	6
2.1	Magnetic forces on electrons in the magnetosphere . . . . .	9
2.2	Contour map of Earth's magnetic field . . . . .	11
2.3	Location of electron beam events . . . . .	12
2.4	Simulation of electron beam and return echo . . . . .	13
2.5	Aligned histogram of electron beam echoes . . . . .	14
3.1	Bayesian Blocks method . . . . .	19
3.2	GUI Map & Event Information . . . . .	22
3.3	GUI Plot . . . . .	23
3.4	Current TGF Catalog Map . . . . .	24
4.1	Stacked histogram of WWLLN strikes . . . . .	30
4.2	Stacked histogram of 14 RHESSI TGFs . . . . .	30

# List of Tables

2.1	Electron beam candidate TGFs . . . . .	13
2.2	Contribution of each TGF to the electron beam signal . . . . .	15
3.1	Stage 1 max probabilities . . . . .	21
3.2	Current optimal thresholds for Stage 2. . . . .	23
3.3	Distribution of events passing current Stage 2 thresholds. . . . .	25

To my parents,  
for 23 years of encouragement in my education,  
and for all of their loving support.

## **Acknowledgements**

I would especially like to thank my thesis advisor, Professor David Smith. The past two years of his encouragement, guidance, and unmatched assistance brought this thesis to full fruition. I would like to acknowledge Dr. Joseph Dwyer, for his electron beam simulations. I wish to also thank Dr. Robert Holzworth for providing the WWLLN data, and Justine Matten for determining which strikes were near RHESSI. Finally, I wish to thank my parents, Michael and Karen Buzbee, my girlfriend Alexis Garcia, and the rest of my friends and family for believing in me and supporting me throughout my education.

# 1 Introduction

Despite how common lightning strikes are, much of the underlying science behind lightning is still unclear due to the extreme complexity involved in the atmospheric discharges. Many aspects of lightning are not understood, including even the trigger mechanism for lightning itself. Atmospheric electricity can take on many forms, including sprites (large red and blue flashes above thunderstorms), ELVES (small, flat and expanding glows extremely high up), and blue jets (blue cone-shaped flashes slightly above the thunderstorm).

One particular form of atmospheric electricity is the terrestrial gamma-ray flash (TGF), a large and sudden burst of gamma-rays. TGFs were discovered offhand by the NASA Burst and Transient Source Experiment (BATSE) on the Compton Gamma-Ray Observatory (CGRO) back in 1994 [12] and were immediately associated with thunderstorms. Soon after, these TGFs were associated with lightning flashes specifically [20], revealing an unknown connection between the two. Originally TGFs were thought to be produced high above stormclouds, much like sprites, but it was later shown that TGFs are produced at storm altitudes [7]. Figure 1.1 shows global maps of detected TGFs and lightning density.

## 1.1 Mechanism of a TGF

Unfortunately, seventeen years later the exact connection between a TGF and lightning is still a mystery, but the picture of how a TGF is formed is beginning to be resolved. Dwyer [10] outlined the process, summarized here.

To begin, we first must consider Fig. 1.2a, showing the force of friction on an electron in air as a function of its energy. We see that above a certain point, the force of friction actually decreases as the electron gains kinetic energy. If the electron has sufficient kinetic energy and is in a strong enough electric field, the force on the electron due to the electric field will be stronger than this force of friction, and the electron will continue to gain kinetic energy. This is called *relativistic runaway*.

A relativistic runaway electron may collide with other electrons, transferring a portion of its kinetic energy to the latter. If the secondary electrons also overcome the frictional force, they will run away as well. Therefore, a single seed electron can create many relativistic electrons, resulting in a *relativistic runaway electron avalanche*. Figure 1.2b shows a result from a Monte Carlo simulation, revealing how a single seed electron can create such an avalanche. Positrons and photons can return to the origin of the avalanche and pair produce or Compton scatter to also create more seed electrons, resulting in many avalanches. Simulations show the number of runaway electrons to be on the order of  $10^{17}$  high-energy electrons [7].

To create relativistic runaway, both a seed particle and sufficiently high electric fields are necessary. Cosmic rays are believed to be the source of the energetic seed particles, and thunderstorms contain sufficiently strong electric fields [10]. A typical thunderstorm has a large central region of negative charge and an upper region of positive charge. This creates an electric field oriented downwards, which would cause an upward force on the negatively-charged electron.

The  $10^{17}$  electrons produced by runaway will therefore be forced to higher altitudes, where they will react with molecules in air. These interactions produce bremsstrahlung. Since the electrons

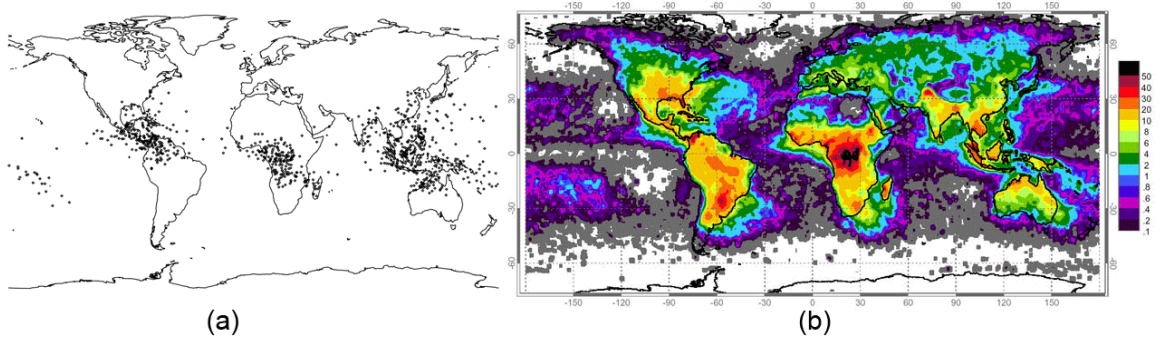


Figure 1.1: (a) Map of subsatellite location for RHESSI TGFs [16]. (b) Global distribution of lightning from April 1995 to February 2003 (NASA's Optical Transient Detector) and January 1998 to February 2003 (NASA's Lightning Imaging Sensor (LIS)) [24]. TGFs occur in areas consistent with lightning activity. However, no TGFs are seen by RHESSI in South America due to the South Atlantic Anomaly (SAA), where high particle precipitation temporarily disables RHESSI.

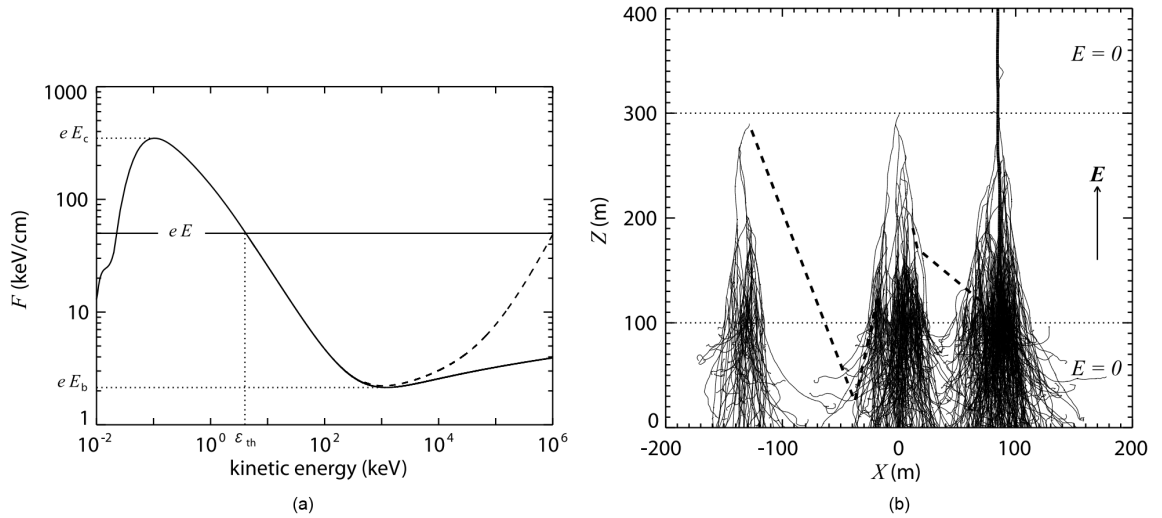


Figure 1.2: (a) Friction force on an electron in air vs its kinetic energy [6]. Runaway occurs when the kinetic energy is greater than  $\varepsilon_{th}$ . (b) Monte Carlo simulation showing a single seed electron causing a relativistic runaway electron avalanche [6].

are extremely energetic, this bremsstrahlung will be in the gamma-ray and x-ray wavelengths. These gamma-rays will be upward, out of the atmosphere. This burst of photons is the terrestrial gamma-ray flash. Figure 1.3 on page 6 shows the geometry of a TGF.

A typical TGF lasts on the order of about 1 ms, and may contain as many as  $10^{17}$  gamma-rays. Currently, it is unknown what the exact connection is between TGFs and lightning strikes, but it is known that not all strikes are associated with TGFs, and thus TGFs cannot be the trigger mechanism of lightning strikes: Smith *et al.* [30] estimate the TGF-to-flash ratio to be between  $10^{-2}$  and  $10^{-3}$ . However, currently all TGFs are believed to be associated with lightning flashes [4], and evidence suggests intracloud lightning (IC) specifically [33].

TGFs also release electron beams [9] – the propagating upward gamma-rays will also interact in the atmosphere via Compton scattering and pair production to release electrons. Although most of these secondary electrons are absorbed, many of those produced sufficiently high in the atmosphere will escape and enter the magnetosphere (see Section 2.1). Because the electrons are captured by the Earth’s magnetic field lines, they are confined to a much smaller region than the propagating cone of gamma rays that form a TGF [9]. Therefore, they are more rarely detected.

## 1.2 RHESSI

Due to the orientation of the electric field, TGFs are mostly detected from space (although they have since been detected from the ground [11] and from aircraft [31]). BATSE had some success in detecting TGFs during its mission [25], but subsequent analyses determined the instrument’s detectors were saturated by TGFs [15], masking many events and their true intensities.

About two years after the deorbit of BATSE, the NASA Reuven Ramaty High Energy Solar Spectroscopic Imager (RHESSI) launched with a primary mission of studying solar flares. RHESSI consists of nine germanium detectors, each divided into front and rear segments. The front segments are oriented towards the sun and are primarily used to study solar flares, but the larger rear segments face the sky, and can detect photons from 25 keV up to 17 MeV [29]. Because RHESSI telemeters most detected photons to the ground, subsequent analyses are possible. RHESSI has had much success in the last eleven years detecting TGFs. The first catalog of RHESSI events contained over eight hundred [16], and a more recent second catalog may more than double that [14].

Figure 1.3 shows the geometry of a TGF relative to RHESSI. By matching lightning sferics (radio noise generated by lightning strikes) to TGFs, the horizontal distance  $x$  to the satellite nadir (the subsatellite point) from a TGF has been consistently found to be mostly within 300km [2] [4] [5] [18]. Such is the intensity of a TGF that RHESSI, an instrument designed to observe energetic solar flares, may be saturated even hundreds of kilometers from the origin [16].

In this paper, we will present three separate topics related to RHESSI and TGFs. First, we present a search for electron beams detected in regions of weaker magnetic field strength relative to the conjugate point. Secondly, we detail a new algorithm to build a third extensive catalog of RHESSI TGF events. Finally, we present the results of summing gamma-ray time profiles associated with flashes recorded by the Worldwide Lightning Location Network (WWLLN) in close proximity to RHESSI to search for sub-luminous TGFs.

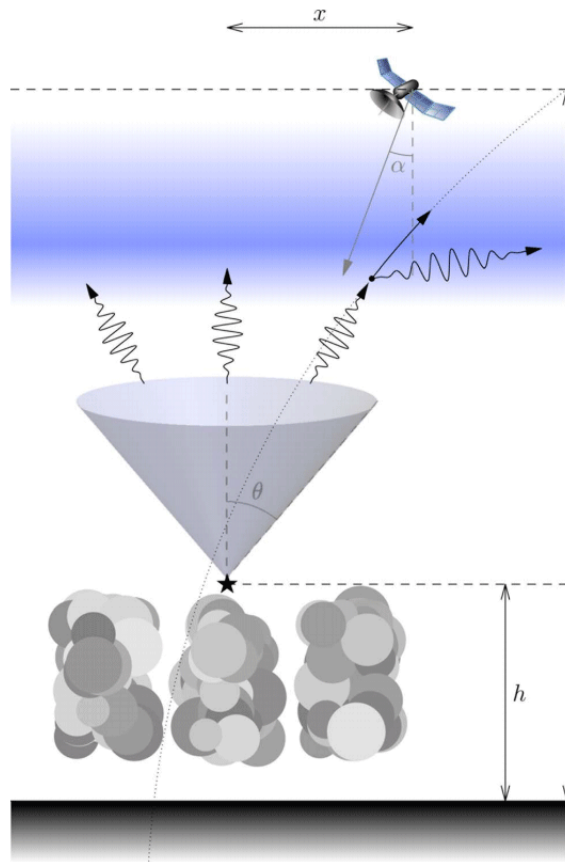


Figure 1.3: Geometry of a TGF event relative to RHESSI (not to scale) [3]. The author notes that the TGF occurs over a volume, and not at a single point. Also, TGFs most likely occur within the cloud, rather than above.

## 2 Electron beam reflections

### 2.1 Introduction: Motion of electrons in the magnetosphere

As previously mentioned, terrestrial gamma-ray flashes emit electron beams in addition to gamma-rays [9]. These electrons enter the Earth's magnetosphere with some pitch angle  $\theta$  relative to a line of the magnetic field. An electron in Earth's magnetic field is subject to the Lorentz force in a magnetic field,  $\mathbf{F} = q(\mathbf{v} \times \mathbf{B})$ . The component of the electron motion perpendicular to the field line causes a radially inward force, and the electrons undergo cyclotron motion around the field line. However, the parallel component of the electron's velocity is undisturbed, and the electron travels parallel to the field line in as it spirals around it. Figure 2.1a shows this motion.

As the electron travels north along the field line and approaches its connection with the Earth, the magnetic field lines begin to converge. This convergence creates a small magnetic field component that points inward radially. By the Lorentz force and the electron's direction of motion around the field line, this force acts opposite the convergence of the field lines, pushing the electron back (Fig. 2.1b). This force can be enough to stop and reverse the electron's motion parallel to the field line, and the electron will mirror along the field line. For the same reasons, the electron will also be repelled at the opposite end of the magnetic field line in the southern hemisphere. Therefore, electrons can oscillate north-to-south along magnetic field lines, as in Fig. 2.1c.

For an electron beam from a TGF, if RHESSI detects the initial beam on its ascent<sup>1</sup>, RHESSI may also detect its reflection as the electrons bounce. This echo is confirmation of the electron beam, and such a reflection has been detected already [9]. This reflection originated at an area of higher magnetic field strength, and so the beam traveled a short distance to the conjugate

<sup>1</sup>Because the electrons travel parallel to the Earth's surface as well, the detection of the initial beam is not necessarily at its origin [9].

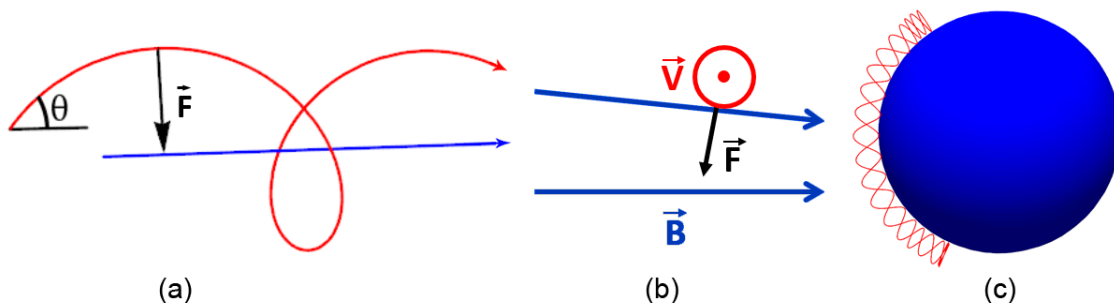


Figure 2.1: (a) Motion of electrons (red) upon entering the magnetosphere. Electrons enter with a pitch angle  $\theta$ , and the radially inward Lorentz force causes cyclotron motion around the magnetic field line (blue). (b) Inward magnetic force on an electron as magnetic field lines converge slows and reverses the electron. (c) Approximation of the mirroring of electrons relative to the Earth.

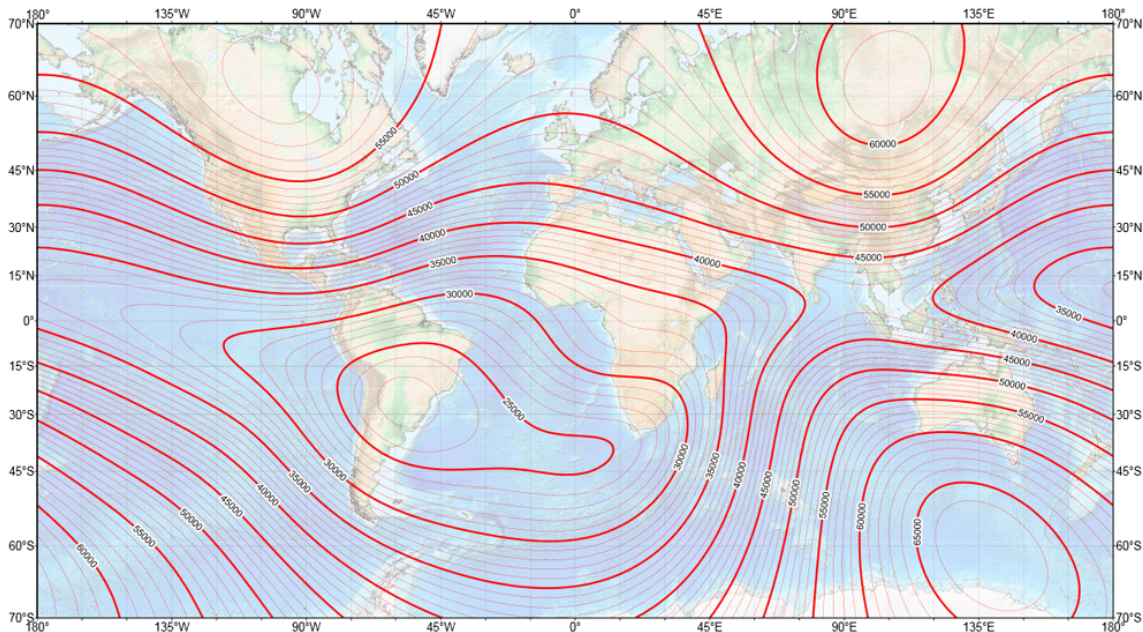


Figure 2.2: Contour map of Earth’s magnetic field intensity [22]. The two zones of weakest field strength over land are located in South America and central Africa.

point before reflecting back to its origin. Our goal is to search for electron beams which are detected in a different region of the electrons’ paths, in an area of *weaker* magnetic field. These electrons will travel a relatively longer distance to the conjugate point before returning to the satellite. To do so, we will search for a returned echo of a TGF.

## 2.2 Methods

### 2.2.1 Restrictions

In order to identify electron beams at the weak magnetic footprint, we first find geographical areas that have a weaker magnetic field relative to their conjugate point. A contour map of Earth’s magnetic field (Fig. 2.2) shows that the continental areas of weakest magnetic field are in South America and central Africa. We search the first TGF catalog by Grefenstette *et al.* [16] for events in these regions<sup>2</sup>. Unfortunately, the area of weakest magnetic field is located at the South Atlantic Anomaly (SAA). In this region, particle precipitation is at a high level due to the low magnetic field, and RHESSI’s detectors are inoperative in this region. Thus, the locations are restricted to  $10^{\circ}$  S -  $15^{\circ}$  N and  $75^{\circ}$  W -  $35^{\circ}$  W for the northern coast of South America, and  $30^{\circ}$  S -  $10^{\circ}$  N and  $0^{\circ}$  E -  $45^{\circ}$  E for southern Africa. These zones are shown in Fig. 2.3.

We also restrict our search to events greater than 1ms in duration. Electrons in an electron beam have a dispersion in pitch angles. These variations in pitch angles lead to differences in electron arrival times: electrons with a smaller pitch angle will arrive slightly sooner than electrons with a larger angle. Long events are not conclusively electron beams, but this eliminates shorter events which must be gamma-rays. We also restrict our search to events containing at least forty counts in the entire burst. Although these large events are not more likely to be electron beams than dimmer

<sup>2</sup>The event in 2012 was not contained in the catalog, but was identified as an electron beam and included in this search.

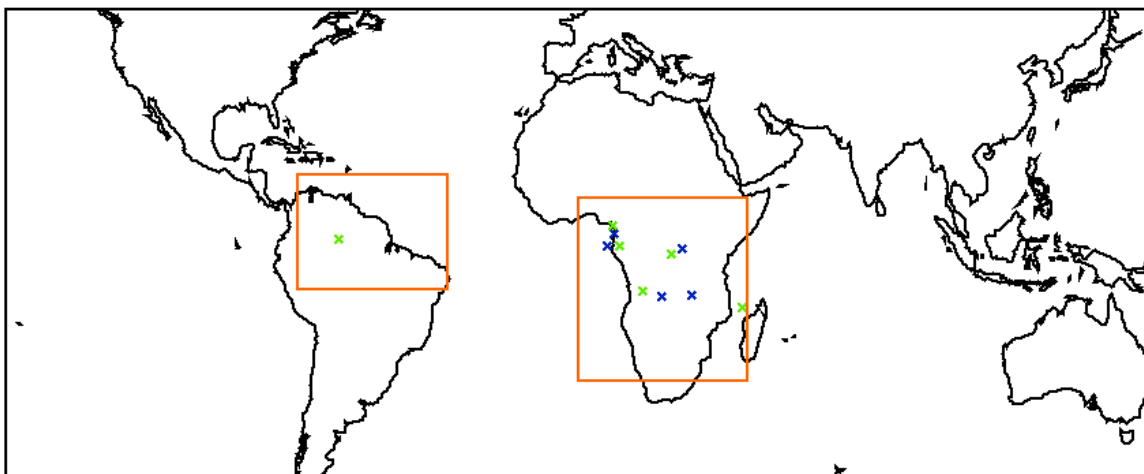


Figure 2.3: Geographic location of the eleven events. The blue X’s correspond to the five events which contributed strongly to the signal, and the green X’s represent the remaining six events. The orange boxes show the boundary zones of the search.

events, they are more likely to have a bright echo, should one exist.

After applying these filters on location, duration, and counts, the events listed in Table 2.1 remain.

### 2.2.2 Simulations

The events listed in Table 2.1 were modeled by Dr. Joseph Dwyer in a Monte Carlo simulation he developed [7]. These simulations incorporate the relevant physics for electrons and photons in air, including Møller scattering, elastic scattering, bremsstrahlung production of high-energy photons, and energy losses via atomic excitation and ionization. The motion of the electrons as they propagate along the magnetic field lines is also simulated, including backscattering, absorption at the conjugate point, and magnetic mirroring [9]. Dr. Dwyer’s simulations calculated the temporal separation between the electron beam’s ascent and its return echo, based on the geographical location of the event. A graphical example of the results of the simulation for the TGF on February 12, 2005 can be seen in Fig. 2.4. Table 2.1 also shows the simulated return time  $\Delta t$  of the electron beam relative to the initial burst, under “Separation”.

### 2.2.3 Stacked alignment

After simulating the duration  $\Delta t$  between the electron beam and its echo, we create a histogram of each TGF’s gamma-ray<sup>3</sup> time profile with a binsize of 1ms. We stack the histograms by summing the histograms for all eleven events, aligned at the calculated return of the echo.

## 2.3 Results

The stacked histogram can be seen in Fig. 2.5. At  $\Delta t = 0$ , the exact point of alignment, a peak is visible. This peak contains 52 counts in one millisecond, compared to the stacked background of 25.978 counts per millisecond. This background was determined from the histogram following the point of alignment, to eliminate the contribution of the TGFs to the background. The Poisson

<sup>3</sup>RHESSI’s detectors cannot discriminate between incoming electrons and gamma-rays.

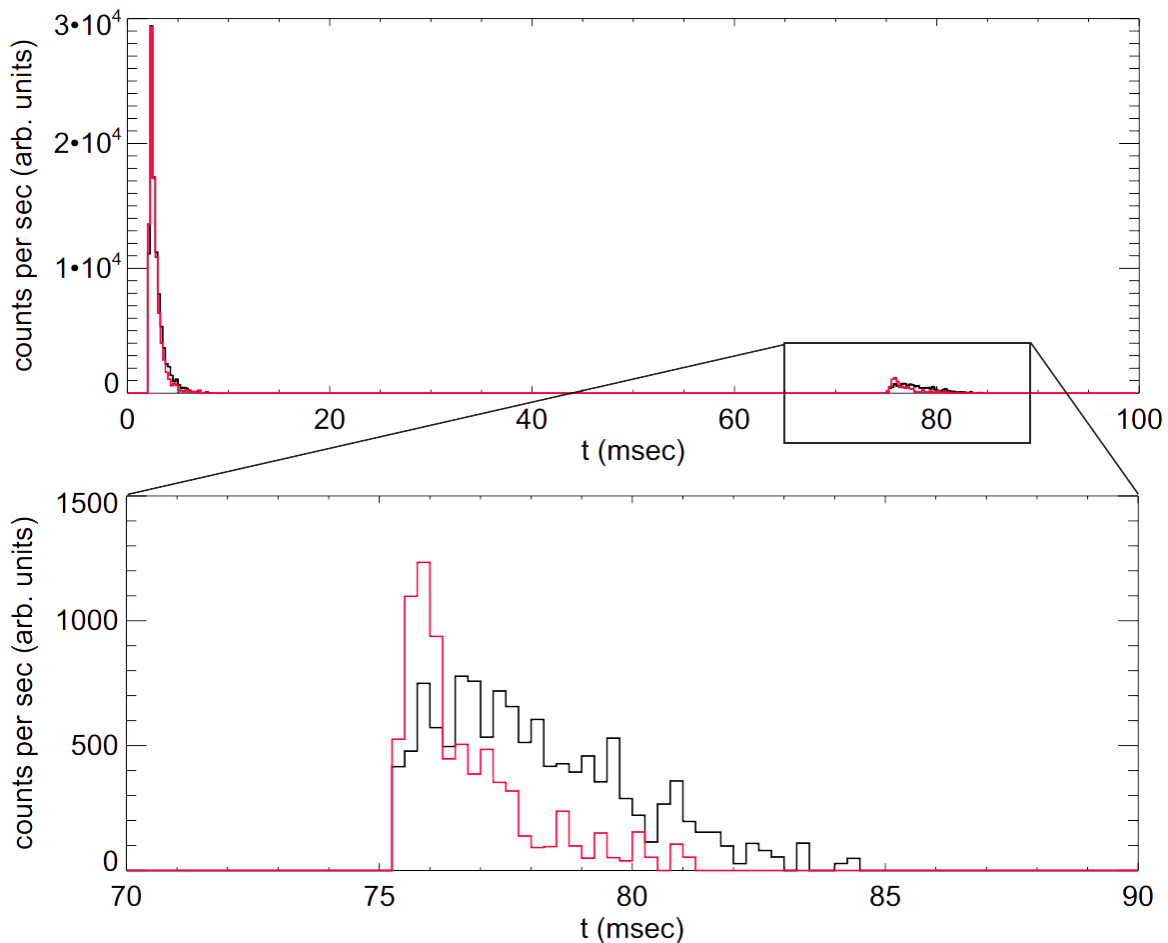


Figure 2.4: Results of Dr. Dwyer's simulation of the TGF/electron beam on February 12, 2005, with its return echo for all electrons (black) and electrons with energies  $\geq 3$  MeV (red). The zoom on the return pulse shows a tightening when only considering high energies.

TGF Timestamp	Latitude ( $^{\circ}$ N)	Longitude ( $^{\circ}$ E)	Duration (ms)	Counts	Separation (ms)
2002-10-18 16:40:14	-2.359	24.877	1.04	45	56
2003-02-23 19:54:07	-0.389	10.972	2.63	44	54
2003-03-23 17:57:01	-10.160	16.976	1.43	71	74
2003-05-17 18:47:01	3.947	9.000	2.93	67	47
2004-03-14 13:44:52	-11.558	22.086	1.53	40	77
2005-02-12 14:59:27	-11.260	30.349	1.81	65	74
2005-03-02 08:00:47	-0.909	27.828	1.02	60	53
2006-03-27 00:12:48	2.290	9.582	1.74	52	49
2007-03-05 22:22:42	-13.976	43.739	1.30	50	80
2007-12-05 06:32:02	-0.447	7.624	1.06	46	54
2012-10-27 22:44:26	0.910	295.905	1.23	82	12

Table 2.1: Eleven electron beam candidates. These eleven TGFs are properly located and of the expected duration, and they are sufficiently bright to allow for a visible echo. The simulated time separation between the TGF and its returned echo are also shown.

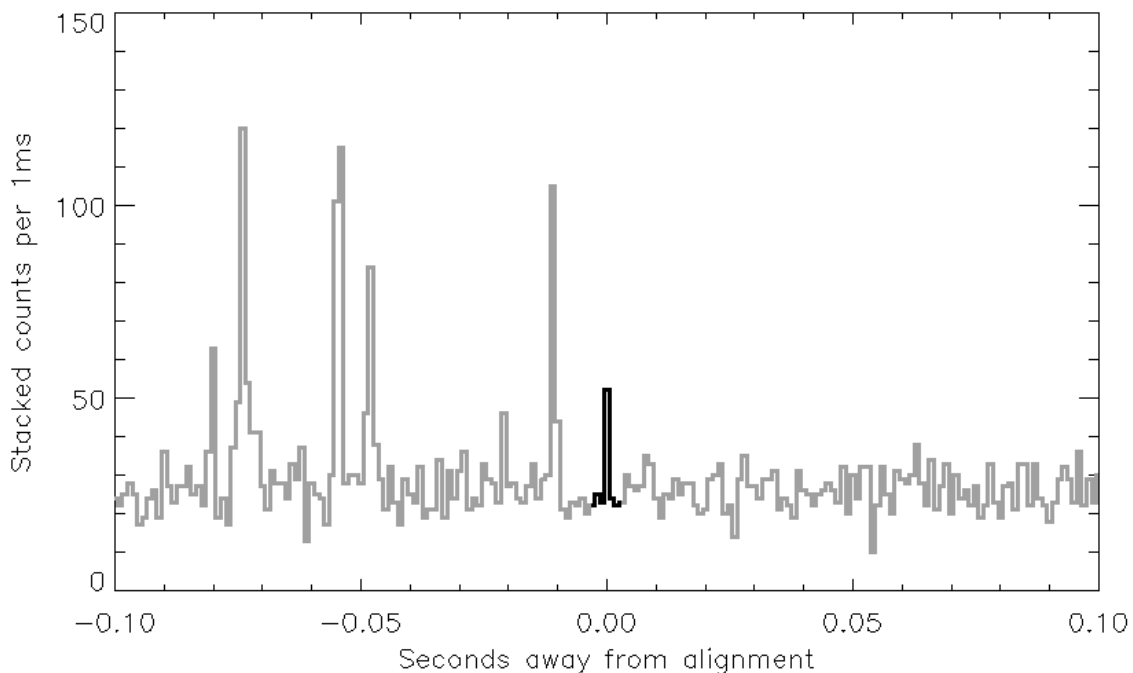


Figure 2.5: A stacked histogram of the electron beam candidate events, aligned at their simulated echo return. The peak at  $\Delta t = 0$  (dark black) has a significance of  $5.1\sigma$ . The large peaks before  $\Delta t = 0$  are due to the stacked TGFs.

probability of detecting at least this number of counts by chance is  $4.53 \times 10^{-6}$ , and lies  $5.1\sigma$  from the mean.

Table 2.2 shows the contribution of each TGF to this signal, along with its individual probability<sup>4</sup> at the bin of alignment. We find that five events in particular, listed first in the table, contributed to this peak. Figure 2.3 on page 12 shows the geographic location of the eleven events. We see that the events which contributed strongly are all located in Africa.

## 2.4 Discussion

The concentration of the return signal into a single millisecond may seem unlikely, but is still consistent with the results of the simulations. The simulation shown in Fig. 2.4 on page 13 shows results for all electrons (black) and only electrons of energy  $\geq 3$  MeV (red). We see that the high-energy electrons have a return pulse which has a peak about 1 ms wide. All electrons lose energy in the satellite’s aluminum body and produce bremsstrahlung, which is detectable by RHESSI’s detectors. However, high-energy electrons produce bremsstrahlung more efficiently than low-energy electrons, and so RHESSI data primarily show the bremsstrahlung of the higher-energy electrons.

We conclude that these five events are the return echoes of electron beam events, showing for the first time a returned electron beam from an area of weaker magnetic field relative to the conjugate point.

---

<sup>4</sup>The event on 2004-03-14 was a double-peaked event, and the initial peak was selected for appending the separation for better alignment. This increases the probability by a factor of two.

TGF Date	Counts at return	Background	Poisson Prob ( $\geq$ bg)
2007-12-05	9	2.94340	0.0033656
2006-03-27	9	3.18982	0.00560
2004-03-14	7	2.35	0.020
2005-03-02	7	2.47534	0.014
2005-02-12	6	2.80	0.065
2003-02-23	3	1.66	0.232
2003-05-17	4	2.96	0.345
2002-10-18	3	2.49	0.454
2007-03-05	1	1.18784	0.695
2012-10-27	1	1.31774	0.73226
2003-03-23	2	2.62	0.736

Table 2.2: The contribution of each event to the electron beam return signal, along with their individual probabilities. The events which contributed most significantly are listed first.

## 3 Building a new RHESSI TGF catalog

### 3.1 Introduction

The first catalog of TGF events observed by RHESSI events was developed in 2008 by Grefenstette *et al* [16], and contained 820 TGFs. The algorithm developed to create the catalog focused on cleanliness over completeness, and utilized strict thresholds. Only events that were particularly prominent and unambiguous met the criteria. In 2012, researchers at the University of Bergen published progress on a new algorithm to identify RHESSI TGFs [14]. This new algorithm had looser thresholds to allow fainter events to trigger as well. Running their algorithm for RHESSI data from 2004 to 2006, they uncovered 1012 events, relative to the original catalog's 472 in the same timeframe – an increase of 114%. This new catalog suggested many fainter events may exist in the RHESSI data.

Our goal is to build a third database to further increase the amount of discovered RHESSI TGFs. Although there may be a high overlap between the catalog built by the University of Bergen, we may find extra events not turned up in either of the other two catalogs. We also wish to search at different timescales for TGFs. TGFs have been observed at small timescales on the order of 100  $\mu\text{s}$  (as discovered by the satellite FERMI [13]), and conjugate electron beams are more visible on timescales greater than 10ms [9]. This catalog will be written in IDL Version 7.1.

### 3.2 Methods

#### 3.2.1 Approach

In order to efficiently create a new catalog of events, the algorithm for finding new TGFs is split into two stages, Stage 1 and Stage 2. Stage 1 is a coarse, breadth-first search which scans relatively quickly through the RHESSI data to identify potential TGF candidates. Stage 2 then examines the triggers from Stage 1 thoroughly to determine whether or not each event is to be considered a TGF.

Both stages are being developed and optimized to search at timescales of 60 $\mu\text{s}$ , 100 $\mu\text{s}$ , 300 $\mu\text{s}$ , 1ms, 3ms, 10ms, and 30ms to find events at any scale.

#### 3.2.2 Stage 1

Since the purpose of Stage 1 is to swiftly scan large amounts of data to identify TGF candidates, Stage 1 is kept relatively simple. Data are broken into four second intervals. A histogram of these data is created, with binsizes corresponding to each timescale. All bins containing more counts than the average are selected, and their Poisson probability of occurring by chance is determined from a previously-created lookup array<sup>1</sup>, given the rate of background within the four second interval. Each probability is compared to a maximum threshold for each timescale. Excesses which are less probable than the threshold are recorded, along with the associated timescale. Stage 1 also

---

<sup>1</sup>For values of  $\lambda > 30$  or  $k > 70$ , a Gaussian approximation is used.

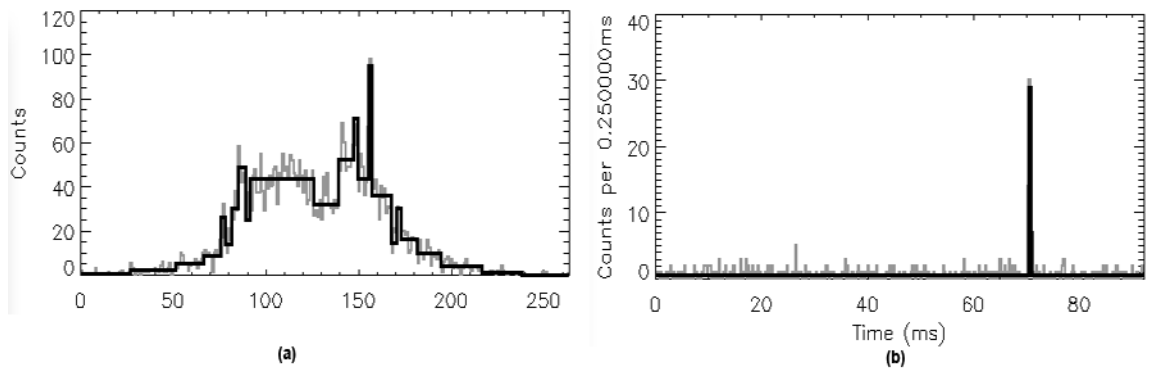


Figure 3.1: (a) 45 random normal distributions stacked and binned using a normal histogram method (gray) and using the Bayesian Blocks method (thick black). The Bayesian method summarizes the important features in the data well. (b) A sample TGF binned using  $250\mu\text{s}$  bins (gray) and Bayesian Blocks (thick black). Most TGFs appear as a single solitary peak with the Bayesian blocks method.

creates a shift of half the timescale and shifts the eventlist before binning a second time – this is to ensure that any events that occur on the edge of adjacent bins are still identified.

Stage 1 also checks that no more than one third of the counts in the entire burst come from any one of RHESSI’s eight functional rear detectors<sup>2</sup>. Real events are likely to appear across most or all detectors, and so this prevents instrumental noise from being falsely triggered on.

Stage 1 can analyze a day’s worth of data in about forty minutes, and therefore will likely analyze the entire RHESSI mission in about one hundred days.

### 3.2.3 Stage 2

First, Stage 2 loads the event list for each trigger from Stage 1, with a buffer of 2.15s on either side of the trigger time. We first check for any attenuator motion. During any attenuator motion, the amount of detected counts skyrockets and can easily be misinterpreted as an event. We also merge coincidences in the event list. Coincidences are multiple near-simultaneous detections in different detectors caused by a Compton scattering photon or by an incident particle depositing energy in several detectors. These coincidences are identified and combined into a single event. Because this process of removing coincidences is relatively time-consuming, it is left to Stage 2.

The algorithm then defines the “peak” specifically. The peak is determined using the method of Bayesian Blocks, described in Scargle *et al.* [28]. The method of Bayesian Blocks creates a histogram with binsizes that adapt to the data (see Fig. 3.1 for an example, both of randomly generated data and a TGF). Because the Bayesian algorithm is also time consuming, only the central 300ms on either side of the trigger time are binned. The peak nearest the trigger time is identified as the peak, but any larger peaks are also analyzed.

For the primary peak and any others, several properties are calculated. These properties are outputted for each peak, to be later analyzed. Each of these properties will later have a threshold placed on it, and only events which pass all of these thresholds will be deemed TGFs.

- **Poisson probability:** The Poisson probability of the peak is again determined, now with coincidences merged. Events must be sufficiently improbable.
- **Distribution of counts:** The standard deviation (second moment) of the spread of photons across the eight rear detectors must be sufficiently high. A small standard deviation implies

<sup>2</sup>One of the nine detectors, Detector 2, is operated at low voltage to avoid arcing, leading to noise [16].

Timescale	Maximum Probability
60 $\mu$ s	$2 \times 10^{-5}$
100 $\mu$ s	$7.3 \times 10^{-5}$
300 $\mu$ s	$2.53 \times 10^{-6}$
1ms	$1.05 \times 10^{-7}$
3ms	$9 \times 10^{-7}$
10ms	$2 \times 10^{-6}$
30ms	$8.8 \times 10^{-7}$

Table 3.1: Current maximum Poisson probabilities for each timescale in Stage 1. Only peaks with Poisson probabilities below their associated threshold will be analyzed by Stage 2.

one detector (or several) received disproportionately many counts, which is characteristic of instrumental noise. A real event will be roughly evenly detected across most or all detectors.

- **Number of counts:** The total number of counts in the TGF must be sufficiently large.
- **Event duration:** TGFs are short events, on the order of a millisecond. Some latitude is given to allow longer and shorter events, particularly at longer timescales.
- **Burst rate:** The “burst rate” is the ratio of number of counts to the event duration. TGFs have a rapid flux of gamma-rays, so events that are too faint are screened out.
- **Background rate:** The average background rate for the event is determined by dividing the total number of counts in the event list by the temporal length of the event list (close to 4.3s).
- **Background consistency:** The relative difference between background rates before and after the peak is calculated. Inconsistent background implies that an edge has been triggered on.

### 3.2.4 Adjusting Thresholds

Adjustment of thresholds in both stages is a must to produce a desired sample of events. The main threshold in Stage 1 to adjust was the maximum Poisson probability for each timescale. These probabilities were adjusted such that each timescale would trigger Stage 1 on about one hundred events per day on average. The current probabilities are listed in Table 3.1.

As mentioned, the Stage 2 thresholds are still under adjustment. Currently, Stage 2 outputs each of the above properties for most events. Weak thresholds are set to vastly reduce the number of items to be analyzed. These light thresholds are set on the number of counts ( $\geq 9$ ), the burst rate ( $> 6$ ), and the probability ( $\leq 10^{-7}$ ). Trial and error along with comparison to the first TGF catalog have shown that the final thresholds on each property will be significantly stricter.

The above properties and a text histogram of each event are outputted and stored such that each threshold can be set retroactively and the effects will quickly be visible. To begin finding an optimal set of thresholds, a quality factor was established to evaluate the fitness of the thresholds. The quality factor was defined as the percentage of triggered events occurring within  $\pm 20^\circ$  latitude. Since most TGFs in the first catalog are observed near the equator (see Fig. 1.1 on page 2), we expect a similar result. Our goal in adjusting the thresholds is to maximize this quality factor when possible.

To assist with optimization, a web GUI was constructed using PHP, JavaScript, the Google Maps API, and MySQL with two main features. The first feature allows quick adjustment of all thresholds, and plots any events which meet all criteria on a Google Maps overlay. These points can be clicked on to bring up a histogram and information about the event (Fig. 3.2). This allows for quick changes to any threshold and visual confirmation of the location of events. Events in

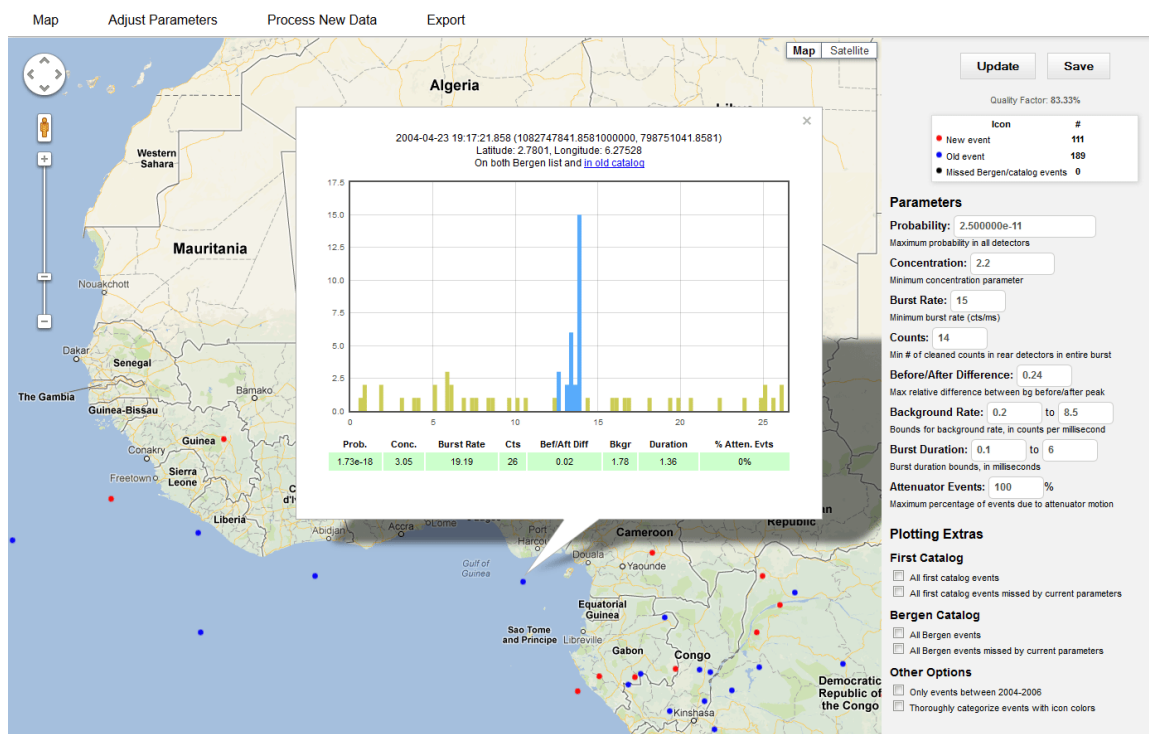


Figure 3.2: Sample web GUI display showing a histogram of a TGF in Africa and its properties. All thresholds are adjustable in the right panel.

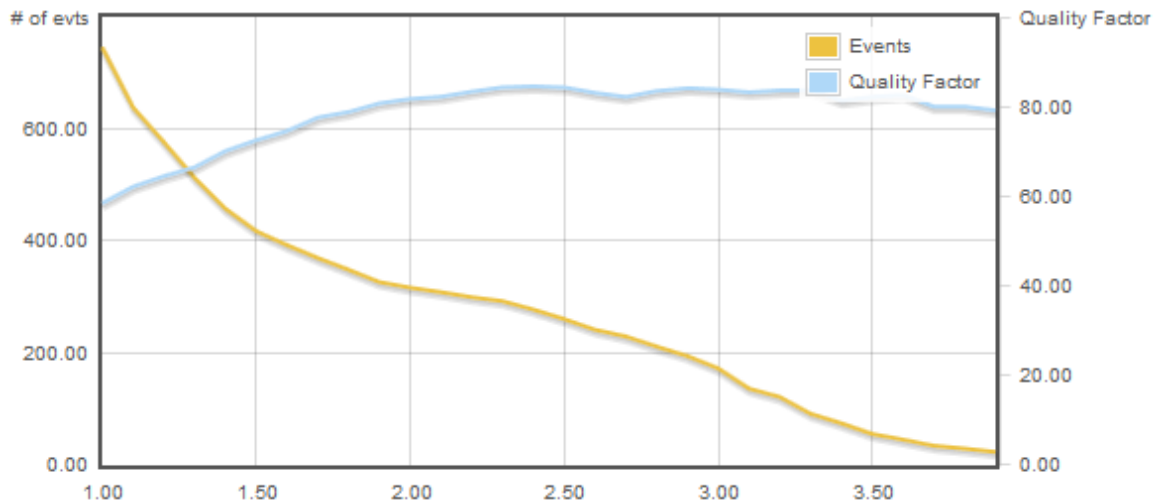


Figure 3.3: Sample web GUI display showing how adjusting the concentration threshold affects the number of events and the quality factor. As the minimum concentration parameter increases, the quality factor increases, but the number of events declines. Using this plot, the current minimum concentration threshold of 2.25 was selected.

Threshold	Minimum	Maximum
Distribution of Counts	2.25	-
Poisson Probability	-	$2.5 \times 10^{-11}$
Number of Counts	14 cts	-
Event Duration	0.1ms	6ms
Burst Rate	15 cts/ms	-
Background Rate	0.2 cts/ms	8.5 cts/ms
Background Consistency	-	0.24

Table 3.2: Current optimal thresholds for Stage 2.

suspicious locations can be analyzed further, leading to improvements in the Stage 2 IDL code or adjustments to thresholds.

The second feature allows for optimization of each threshold by running a simple `for` loop on any of the parameters while keeping the others fixed. A plot is outputted presenting the number of events passing that threshold and the corresponding quality factor, as shown in Fig. 3.3. Using the plot, a suitable threshold could be chosen for each parameter that allowed for an ideal balance between number of events and the quality factor. Each threshold was set in order in an initial loop, and then refined in a second loop to give the current thresholds in Table 3.2.

### 3.3 Results

Currently, 627 days have been analyzed entirely by Stage 2. These 627 days are dispersed evenly throughout the RHESSI mission from 2002 to 2013. 297 events have passed all current thresholds. Figure 3.4 shows a map of these events. The events are distributed in locations consistent with the previous two RHESSI catalogs: in Central America, southern Africa, and the Asian Pacific. This consistency suggests that our thresholds are realistic.

189 of these events are “old” events which were in one or both of the previous two catalogs,

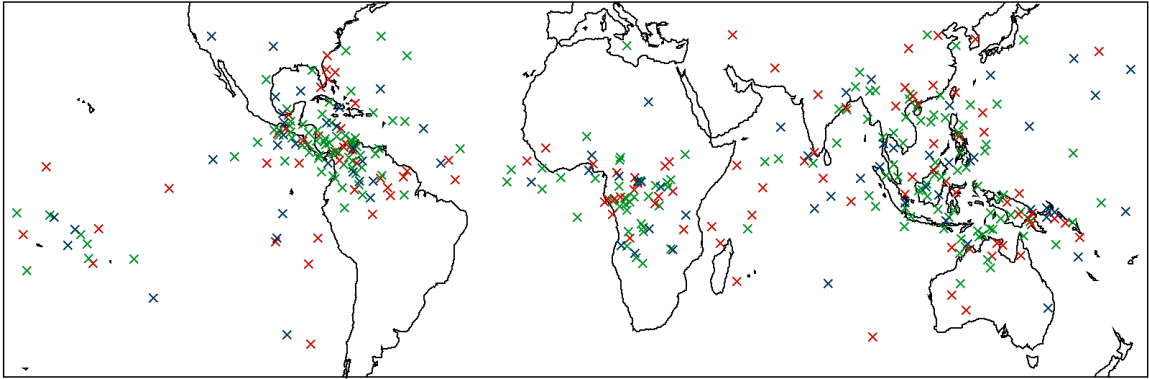


Figure 3.4: Map of events passing current TGF parameters. “Old” events in either previous catalog that passed all thresholds are denoted by green, “new” events are denoted by red, and missed old events are denoted by blue diamonds.

<b>New Events</b>	<b>108</b>
- 2004-2006	19
<b>Confirmed Old Events</b>	<b>189</b>
- Grefenstette Catalog	157
- Bergen Catalog	80
<b>Missed Old Events</b>	<b>76</b>
- Grefenstette Catalog	35
- Bergen Catalog	41

Table 3.3: Distribution of events passing current Stage 2 thresholds.

and 108 are new. Table 3.3 provides counts of the distribution of these events and comparisons to the two previous catalogs. It’s worth note that the Bergen catalog only contains events between 2004 and 2006, whereas this analysis was ran from across the past ten years.

## 3.4 Discussion

When comparing the results between 2004 and 2006, we find only 19 new events, compared to missing 41 from the Bergen catalog. We also find that 35 events from the Grefenstette catalog were not triggered on. Because the Grefenstette catalog contains only the most significant events, this suggests that further refinement and debugging is necessary. It is possible that some events in the previous two catalogs were false positives, but it is much more likely that further work remains to be done.

The most suspect cause for the missed events is the output of the Bayesian Blocks algorithm. Although the method is a powerful tool for finding and defining prominent features quickly, some events may fall through the cracks or be misinterpreted.

### 3.4.1 Future Work

The primary remaining goal is to identify the discrepancies between this new algorithm and the two previous catalogs. Adjustments to the Bayesian method or the Stage 2 thresholds will hopefully bring the three catalogs closer into agreement, while still yielding new events.

Continuing to analyze data from throughout the RHESSI mission will also assist in optimizing the chosen thresholds by continuing to investigate individual events which pass or fail the thresholds. Events clustered in isolated regions have revealed necessary improvements to make to all parts of the IDL code in Stage 1 and Stage 2. Further analysis into similar clusters will hopefully continue to yield the same insight. We also intend to search for WWLLN lightning strikes that can be associated with TGFs in these regions, for evaluation of our algorithm. We hope to determine our rate of false positives.

Finally, once all parameters are properly adjusted, this new algorithm can be ran on the entire RHESSI mission to build a third catalog of events, open for further analysis. A final interactive map of events in the catalog will also be created and released to the world.

## 4 Using WWLLN to search for sub-luminous TGFs

### 4.1 Introduction

In lowering and optimizing our thresholds, many more RHESSI TGFs were revealed. However, these limits can only be loosened to a certain point, after which false detections (noise) increase. Yet there may still exist TGFs of weaker intensities. TGFs may follow a power law distribution, like many other physical processes, including earthquakes [17] and moon craters [26]. In a power law distribution, the probability of the fluence of events  $x$  is distributed as  $p(x) = Cx^{-\lambda}$ , where  $\lambda > 1$ . Other physical events, such as earthquakes and solar flares, Recent studies have estimated that TGFs follow a power law distribution with  $\lambda = 2.3 \pm 0.2$  [27]. How far down this distribution extends and its behavior are yet to be determined, but if TGFs do follow a power-law distribution, there may be very many sub-luminous events, not individually detectable from satellite altitudes.

However, by stacking and aligning the light curve of an adequate number of events, a statistically significant excess could emerge, even if the average flux detected by RHESSI per event is less than one photon. The challenge comes in determining when to look, as searching a random sample of times will not produce a result above noise. Since TGFs are known to be associated with lightning [20], searching at times of lightning strikes is appropriate.

By using sferic data from the World Wide Lightning Location Network (WWLLN) [19], a network of lightning sensors directed by Dr. Robert Holzworth, we can determine which flashes were in close proximity to RHESSI. By again aligning and stacking the gamma-ray time profiles of these strikes, we can determine whether or not such a population exists.

### 4.2 Methods

#### 4.2.1 Finding Nearby Strikes

The database of WWLLN flashes for 2008, 2011, and 2012 was analyzed by Justine Matten to determine their proximity to RHESSI. Events within 500km were listed together for further analysis. Data on flash intensity and distance were preserved for subsequent analyses.

#### 4.2.2 Processing RHESSI data

After identifying the WWLLN events near RHESSI, we then tried to determine at what point photons from the flash would reach RHESSI. The horizontal distance from the flash to RHESSI is determined by using the great circle method

$$d_h = R_{\oplus} \cos^{-1} [\sin \phi_R \sin \phi_F + \cos \phi_R \cos \phi_F \cos (\lambda_R - \lambda_F)] \quad (4.1)$$

where  $\phi$  denotes the longitude and  $\lambda$  denotes the latitude, and the subscript  $F$  denotes the coordinates of the flash, and  $R$  of RHESSI.  $R_{\oplus}$  denotes the radius of Earth. After determining the horizontal distance, we determine the total distance from each flash to RHESSI using the Pythagorean

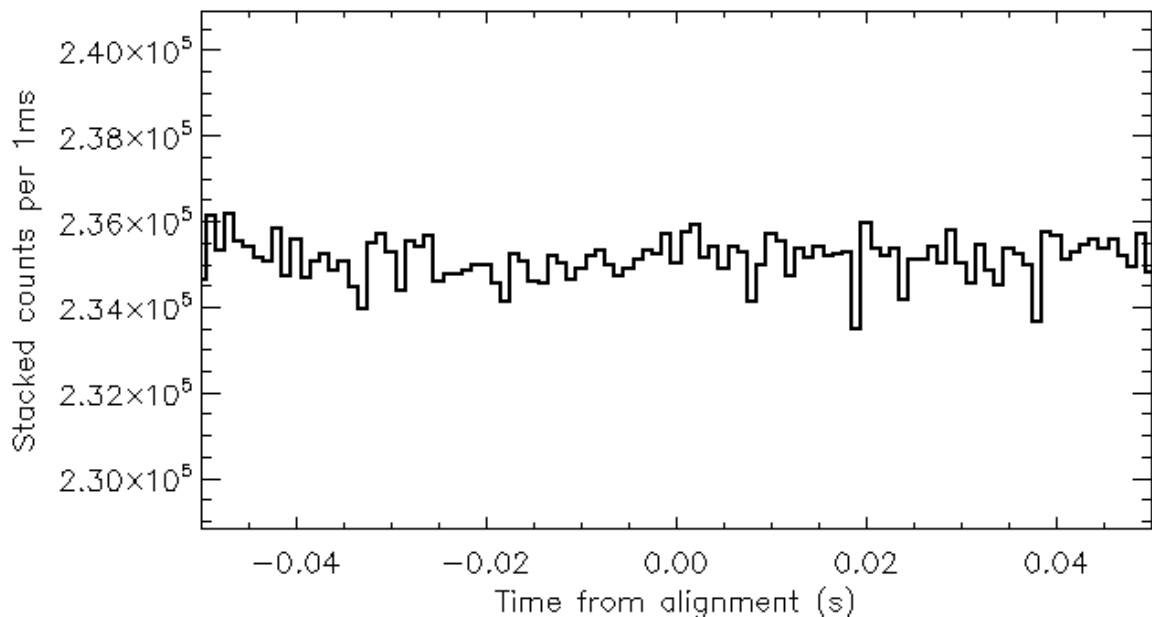


Figure 4.1: A stacked histogram of all WWLLN strikes within 300km of RHESSI in 2008, 2011, and 2012. No central excess exists at the point of alignment.

theorem as

$$D = \sqrt{d_h^2 + (z - 15)^2}. \quad (4.2)$$

Here, RHESSI's altitude at the time is given by  $z$ , and we make the assumption that the altitude of each flash is 15km, the approximate altitude of a typical thunderstorm. Using this net distance to the satellite, we account for the travel time of the light by  $t = \frac{D}{c}$  to predict the time at which photons from the strike would reach the satellite. We also subtract a clock correction of  $1.8\text{ms}^1$ .

After predicting the arrival time of photons, the RHESSI event list for each strike is processed, and coincidences are merged, as in the creation of the TGF catalog. The event list is then binned to one millisecond. As with the search for electron beam echoes, these histograms are stacked and aligned at the expected photon arrival time.

Different stacked histograms were created after applying thresholds to the energy of the flashes and their proximity to RHESSI<sup>2</sup>.

### 4.3 Results

A plot of the histogram for all strikes within 300km of RHESSI over the three years can be seen in Fig. 4.1. We see that, for these lightning strikes, no significant excess exists. By comparison, aligning and stacking the eventlists for fourteen RHESSI TGFs produces a large peak as shown in Fig. 4.2.

<sup>1</sup>This clock correction originates from a time discrepancy between separate observations of magnetar SGR 1806-20 [16]. This correction should not be considered exact.

<sup>2</sup>For these thresholds, we use the horizontal distance between the flash and the RHESSI nadir, and not the net distance to the satellite.

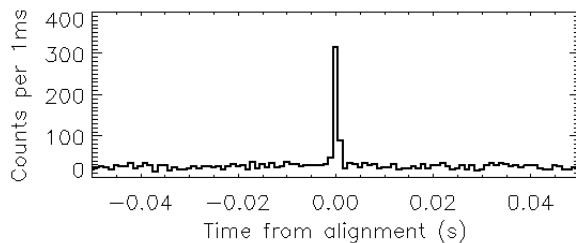


Figure 4.2: A stacked histogram of 14 RHESSI TGFs, aligned using an identical method used to align the WWLLN strikes. These 14 TGFs produce a prominent peak.

## 4.4 Discussion

The stacked histograms created with thresholds on energy and radius also showed no excesses. The absence of any excess implies that either no large population of sub-luminous TGFs exists, or that it is too weak to be detected by RHESSI.

However, we can still establish a strong upper limit on the average gamma-ray flux associated with lightning. We use the values in the central alignment bin and one bin on either side, for a total of 3 ms, as our average value for the gamma-rays associated with the lightning strikes,  $I$ . The error on this is  $\sigma_I = \sqrt{N_I}/N$ , where  $N_I$  is the total number of counts in the central three bins of the stacked histogram, and  $N$  is the total number of distinct light curves summed in the histogram.

We determine the average background,  $bk_g$ , from each stacked histogram to be the average value in the bins that are 10 to 100 bins out on both sides of the alignment. Since we are comparing it to the central three bins, we multiply this average by three. The error on this background is given by

$$\sigma_{bk_g} = \frac{3}{182} \times \frac{\sqrt{N_{bk_g}}}{N}, \quad (4.3)$$

where  $N_{bk_g}$  is the sum of all counts within the background bins. We divide by 182, the number of bins used to determine background, and multiply by three to scale our error to 3ms as well. Again, we divide by  $N$ . We then subtract the background rate  $bk_g$  from the central flux  $I$  to obtain a value with background removed,  $S = I - bk_g$ . The error on this subtracted value  $\sigma_S$  is then simply the errors on  $bk_g$  and  $I$  added in quadrature, given by

$$\sigma_S = \sqrt{\sigma_{bk_g}^2 + \sigma_I^2}. \quad (4.4)$$

With 95% confidence, we can express this as an upper-limit of gamma-ray flux associated with lightning as seen by RHESSI by adding  $1.96 \times \sigma_S$  to our subtracted value. If we divide by the amount of counts in an average TGF seen by RHESSI (which we define to be 25 counts), we can express this upper-limit as a fraction of a TGF per each flash as

$$U_{95\%} = \frac{S + 1.96\sigma_S}{25}. \quad (4.5)$$

However, TGFs are associated with intracloud (IC) lightning [32], and so our sample is diluted by the cloud-to-ground (CG) flashes. Since WWLLN does not provide information about whether a strike was IC or CG, we refer to Abarca *et al.* [1] which suggests that WWLLN's detection efficiency of IC strikes ( $\varepsilon_{IC}$ ) is about 45% that of its efficiency of detecting CG strikes ( $\varepsilon_{CG}$ ).

Mackerras *et al.* [21] also showed that the ratio of IC to CG strikes,  $z$ , varies by latitude. From  $0^\circ$  -  $20^\circ$ ,  $z$  was measured to be 3.96. From  $20^\circ$  -  $40^\circ$ ,  $z$  was measured at 3.18. Since the peak latitudes of RHESSI's orbit are within  $40^\circ$  and about 52% of the nearby WWLLN flashes fell within

$20^\circ$  of the equator, we average the two values of  $z$  to obtain  $z = 3.57$ . Therefore, the probability that a given WWLLN flash is IC is given by:

$$P_{IC} = \frac{N_{IC}\varepsilon_{IC}}{N_{CG}\varepsilon_{CG} + N_{IC}\varepsilon_{IC}}$$

$$P_{IC} = \frac{0.45z}{1 + 0.45z}$$

$$P_{IC} \approx 0.6163$$

Our upper limits must then be divided by this probability to account for the CG dilution.

Previous studies associating RHESSI TGFs with lightning strikes have found that most TGFs detected by RHESSI are within 300km of RHESSI nadir [2] [4] [5] [18]. Thus, in setting our upper-limit, we restrict our flashes to those within 300km of RHESSI. We arrive on an upper limit of gamma-ray flux per stroke of  $6.20 \times 10^{-4}$  of an average RHESSI TGF, with 95% confidence.

## 5 Conclusions

In this paper, we presented three separate analyses of RHESSI data related to TGFs.

We first found confirmation of five electron beam events on the weak end of a magnetic field line by detecting their reflection. By finding TGFs located in suitable regions and of sufficient duration and luminosity, we used simulations to calculate the return time. Creating a stacked histogram at this time revealed a central peak of significance  $5.1\sigma$  at the exact point of alignment. Five of the eleven candidates contributed strongly to this signal, and we conclude that these events are the first detected electron beams at the weak point of a magnetic field line.

Secondly, we presented the current progress on efforts to build a third extensive RHESSI TGF catalog. Currently, 108 new events have been detected, yet 76 older events were untriggered. Future analysis will hopefully resolve the remaining discrepancies.

Finally, we found no evidence for a large population of sub-luminous TGFs after analyzing RHESSI gamma-ray time profiles associated with WWLLN lightning flashes. We conclude that no population detectable by RHESSI exists, and set an upper-limit on the gamma-ray flux from lightning detected by RHESSI to be  $6.20 \times 10^{-4}$  of an average RHESSI TGF.

# Bibliography

- [1] Abarca, S. F., K. L. Corbosiero, and T. J. Galarneau Jr. (2010), An evaluation of the Worldwide Lightning Location Network (WWLLN) using the National Lightning Detection Network (NLDN) as ground truth, *J. Geophys. Res.*, *115*, D18206, doi:10.1029/2009JD013411.
- [2] Cohen, M. B., U. S. Inan, R. K. Said, and T. Gjestland (2010), Geolocation of terrestrial gamma-ray flash source lightning, *Geophys. Res. Lett.*, *37*, L02801, doi:10.1029/2009GL041753.
- [3] Collier, A. B., T. Gjestland, and N. Østgaard (2011), Assessing the power law distribution of TGFs, *J. Geophys. Res.*, *116*, A10320, doi:10.1029/2011JA016612.
- [4] Connaughton, V., et al. (2010), Associations between Fermi Gamma-ray Burst Monitor terrestrial gamma ray flashes and sferics from the World Wide Lightning Location Network, *J. Geophys. Res.*, *115*, A12307, doi:10.1029/2010JA015681.
- [5] Cummer, S. A., Y. Zhai, W. Hu, D. M. Smith, L. I. Lopez, and M. A. Stanley (2005), Measurements and implications of the relationship between lightning and terrestrial gamma ray flashes, *Geophys. Res. Lett.*, *32*, L08811, doi:10.1029/2005GL022778.
- [6] Dwyer, J. R., et al. (2003), Energetic radiation produced during rocket-triggered lightning, *Science*, *299*, 694697, doi:10.1126/science.1078940
- [7] Dwyer, J. R., and D. M. Smith (2005), A comparison between Monte Carlo simulations of runaway breakdown and terrestrial gamma-ray flash observations, *Geophys. Res. Lett.*, *32*, L22804, doi:10.1029/2005GL023848.
- [8] Dwyer, J. R. (2007), Source mechanisms of terrestrial gamma-ray flashes, *J. Geophys. Res.*, *113*, D10103, doi:10.1029/2007JD009248.
- [9] Dwyer, J. R.; Grefenstette, B. W.; Smith, D. M. (2008), High-energy electron beams launched into space by thunderstorms, *2008GeoRel..3502815D*, *35*, 2815, doi:10.1029/2007GL032430
- [10] Dwyer, J. R. (2012), The relativistic feedback discharge model of terrestrial gamma ray flashes, *J. Geophys. Res.*, *117*, A02308, doi:10.1029/2011JA017160
- [11] Dwyer, J. R., M. M. Schaal, E. Cramer, S. Arabshahi, N. Liu, H. K. Rassoul, J. D. Hill, D. M. Jordan, and M. A. Uman (2012), Observation of a gamma-ray flash at ground level in association with a cloud-to-ground lightning return stroke, *J. Geophys. Res.*, *117*, A10303, doi:10.1029/2012JA017810.
- [12] Fishman, G. J.; Bhat, P. N.; Mallozzi, R.; et al. (1994), Discovery of Intense Gamma-Ray Flashes of Atmospheric Origin, *Science*, New Series, Vol. 264, No. 5163 (May 27, 1994), 1313-1316.

- [13] Fishman, G. J., *et al.* (2011), Temporal properties of the terrestrial gamma-ray flashes from the Gamma-Ray Burst Monitor on the Fermi Observatory, *J. Geophys. Res.*, *116*, A07304, doi:10.1029/2010JA016084.
- [14] Gjesteland, T., N. Østgaard, A. B. Collier, B. E. Carlson, C. Eyles, and D. M. Smith (2012), A new method reveals more TGFs in the RHESSI data, *Geophys. Res. Lett.*, *39*, L05102, doi:10.1029/2012GL050899.
- [15] Grefenstette, B. W., D. M. Smith, J. R. Dwyer, and G. J. Fishman (2008), Time evolution of terrestrial gamma ray flashes, *Geophys. Res. Lett.*, *35*, L06802, doi:10.1029/2007GL032922.
- [16] Grefenstette, B. W., D. M. Smith, B. J. Hazelton, and L. I. Lopez (2009), First RHESSI terrestrial gamma ray flash catalog, *J. Geophys. Res.*, *114*, A02314, doi:10.1029/2008JA013721.
- [17] Gutenberg, B., Richter, C. F. (1945), Frequency of Earthquakes in California, *Bulletin of the Seismological Society of America*, *34*, 185-188.
- [18] Hazelton, B. J., *et al.* (2009), Spectral dependence of terrestrial gamma-ray flashes on source distance, *Geophys. Res. Lett.*, *36*, L01108, doi:10.1029/2008GL035906.
- [19] Hutchins, M. L., R. H. Holzworth, J. B. Brundell, and C. J. Rodger (2012), Relative detection efficiency of the World Wide Lightning Location Network, *Radio Sci.*, *47*, RS6005, doi:10.1029/2012RS005049.
- [20] Inan, S. U., S. C. Reising, G. J. Fishman, and J. M. Horack (1996), On the association of terrestrial gamma-ray bursts with lightning and implications for sprites, *Geophys. Res. Lett.*, *23*, 10171020.
- [21] Mackerras, D., and M. Darveniza (1994), Latitudinal variation of lightning occurrence characteristics, *J. Geophys. Res.*, *99(D5)*, 1081310821, doi:10.1029/94JD00018.
- [22] Maus, S., S. Macmillan, S. McLean, B. Hamilton, A. Thomson, M. Nair, and C. Rollins, 2010, The US/UK World Magnetic Model for 2010-2015, NOAA Technical Report NESDIS/NGDC.
- [23] Moss, G., V. P. Pasko, N. Liu, and G. Veronis (2006), Monte Carlo model for analysis of thermal runaway electrons in streamer tips in transient luminous events and streamer zones of lightning leaders, *J. Geophys. Res.*, *111*, A02307, doi:10.1029/2005JA011350
- [24] NASA MSFC Lightning (2004), Worldwide Lightning Strikes, [http://www.nasa.gov/centers/goddard/news/topstory/2004/0621lightning\\_prt.htm](http://www.nasa.gov/centers/goddard/news/topstory/2004/0621lightning_prt.htm), Retrieved April 1, 2013.
- [25] Nemiroff, R. J., J. T. Bonnell, and J. P. Norris (1997), Temporal and spectral characteristics of terrestrial gamma flashes, *J. Geophys. Res.*, *102(A5)*, 96599665, doi:10.1029/96JA03107.
- [26] G. Neukum and B.A. Ivanov, in Hazards Due to Comets and Asteroids, edited by T. Gehrels (University of Arizona Press, Tucson, AZ, 1994), pp. 359416.
- [27] Østgaard, N., T. Gjesteland, *et al.* (2012), The true fluence distribution of terrestrial gamma flashes at satellite altitude, *J. Geophys. Res.*, *117*, A03327, doi:10.1029/2011JA017365.
- [28] Scargle, J, *et al.* (2013), Studies in Astronomical Time Series Analysis. VI. Bayesian Block Representations, *The Astrophysical Journal*, *764*, 167, doi:10.1088/0004-637X/764/2/167
- [29] Smith, D. M., *et al.* (2002), The Rhessi Spectrometer, *Solar Physics*, *2010*, 0038-0938, doi:10.1023/A:1022400716414

- [30] Smith, D. M.; Dwyer, J. R.; Hazelton, B. J.; et al. (2011), The rarity of terrestrial gamma-ray flashes, *2011GeoRL..3808807S*, 38, 8807, doi:10.1029/2011GL046875
- [31] Smith, D. M., et al. (2011), A terrestrial gamma ray flash observed from an aircraft, *J. Geophys. Res.*, 116, D20124, doi:10.1029/2011JD016252.
- [32] Stanley, M. A., X.-M. Shao, D. M. Smith, L. I. Lopez, et al. (2006), A link between terrestrial gamma-ray flashes and intracloud lightning discharges, *Geophys. Res. Lett.*, 33, L06803, doi:10.1029/2005GL025537.
- [33] Williams, E., et al. (2006), Lightning flashes conducive to the production and escape of gamma radiation to space, *J. Geophys. Res.*, 111, D16209, doi:10.1029/2005JD006447.